Anharmonic model for the elastic constants of bulk metallic glass across the glass transition

Zachary H. Aitken,[1,*] Mehdi Jafary-Zadeh,[1] John J. Lewandowski,[2] and Yong-Wei Zhang[1]
[1]*Institute of High Performance Computing, A*STAR 1 Fusionopolis Way, #16-16 Connexis, Singapore 138632, Singapore*
[2]*Department of Materials Science and Engineering, Case Western Reserve University, Cleveland, Ohio 44106, USA*

(Received 12 July 2017; revised manuscript received 21 September 2017; published 9 January 2018)

Here we examine the role of anharmonicity in the elastic constants of bulk metallic glasses and develop an anharmonic model to consider the effects of both pressure and temperature across the glass transition. By comparing against reported experimental data and elastic constants obtained from molecular dynamics simulations, we show that the model is able to capture reported elastic constants from cryogenic temperatures through the glass transition and under hydrostatic pressures up to 18 GPa. Microstructural indicators based on short-range order analysis also display strong correlations with the bulk and shear moduli across the range of pressures and temperatures studied. These results not only greatly expand our understanding in the physical origins of elastic properties of bulk metallic glasses but are also of practical interest for application to processing routes for bulk metallic glass materials.

DOI: 10.1103/PhysRevB.97.014101

I. INTRODUCTION

Bulk metallic glasses (BMGs) include systems with varied chemistry and can display high strength, low weight, and excellent fracture toughness [1–4]. However, due to their tensile brittleness in bulk form arising from localized deformation, processing MGs at room temperature or lower is still a significant challenge. It is known that within the solid glassy regime, BMGs generally display decreasing strength and elastic moduli with increasing temperature and an accompanying shift from brittle failure in tension (localized shear deformation) to increasing tensile ductility (homogeneous deformation) [5–7]. These changes may thus present a viable window for processing BMGs. Further increasing temperature beyond the glass transition temperature leads to supercooled liquid behavior where the viscosity of the metallic alloy decreases by several orders of magnitude and processing BMGs under thermoplastic forming may be also viable [8,9]. Clearly, the temperature-dependent mechanical and viscous behavior of BMGs serves as a key to unravel the still-mysterious glass transition phenomenon and identify processing windows for BMGs [10].

Previous studies have indicated that BMGs tend to display a weak sensitivity to hydrostatic pressure at temperatures well below T_g [11–15]. However, recent tension and compression experiments conducted at a significant fraction of the glass transition temperature revealed that the mechanical response of BMGs displays increasing hydrostatic pressure dependence. For example, Vatamanu *et al.* reported that tension and compression experiments on Zr and La-based BMGs performed at temperatures between 70% and 90% of the glass transition temperature showed a significant increase in fracture stress as well as a transition from homogeneous deformation to localized failure when a hydrostatic pressure was applied [16]. Other reported effects of hydrostatic pressure include an increase in the glass transition and crystallization temperature with pressure [17,18], an anomalous energy-density relation under simulated pressure quenching [19], and high-pressure amorphous to amorphous phase transition [20]. Given the importance of understanding the fundamental physics during the glass transition and developing practical thermoplastic processing techniques, understanding the pressure sensitivity of the mechanical properties near the glass transition becomes imperative and necessary.

Current models for the temperature dependence of the elastic properties of BMGs rarely approach the glass transition regime. To our knowledge, currently, there is no theory that is able to simultaneously capture temperature- and pressure-dependent behavior in the elastic properties of BMGs. Clearly, a physically grounded model that is able to capture both effects will not only be able to contribute to understanding these observed phenomena and underlying physics, but also revealing practical routes for processing BMGs.

Our above discussion highlights several areas of interest regarding the effect of pressure on the mechanical properties and microstructure of a BMG across a wide temperature range. Incorporating the effects of pressure and temperature through the glass transition regime will not only provide a theoretical basis for temperature-dependent pressure sensitivity, but also suggest new thermodynamic pathways in controlling the mechanical behavior of a BMG and further identify practical processing windows for BMGs. In this paper, we propose a model based on anharmonic theory to capture both temperature- and pressure-dependence in the mechanical properties of BMGs. We validate this model with several experimental data and the results from molecular dynamic simulations.

II. MODEL

The pressure and temperature dependence of properties such as the elastic constants is known to arise from

*zach-aitken@ihpc.a-star.edu.sg

anharmonicity of the interatomic potential [7,21]. Using a quasiharmonic approximation, the adiabatic elastic constants can be expressed using the following general form [21]:

$$C^{ad}_{ik,jl} = \tilde{C}_{ik,jl}(1 - D_{ik,jl}\bar{\epsilon} + d_{ik,jl}P). \quad (1)$$

$\tilde{C}_{ik,jl}$ is the harmonic contribution to the elastic modulus, $\bar{\epsilon}$ is the mean energy per oscillator, and P is an external hydrostatic pressure. $D_{ik,jl}$ and $d_{ik,jl}$ are assumed constant within the quasiharmonic approximation. Equation (1) shows the temperature dependence of the elastic constants through the mean energy per oscillator, $\bar{\epsilon}$, and the pressure dependence through the term linear with pressure. Following the assumptions of the Einstein model and taking the system as individual harmonic oscillators, it can be shown that $\bar{\epsilon} = \frac{1}{2}h\nu + \frac{h\nu}{e^{h\nu/kT}-1}$, where h is Planck's constant, ν is the oscillation frequency, and k is Boltzmann's constant. For the case with no applied pressure ($P = 0$), Eq. (1) then gives the functional form of the Varshni expression. The empirical Varshni model was originally proposed to provide an accurate model for the behavior of the elastic constants from room temperature down to near absolute zero for a wide range of materials, including crystalline metals, intermetallic compounds, and crystalline benzene [22]. More recently, it has been used effectively to model the temperature dependence of many BMGs at low temperatures [23–27].

From the above discussion, a reasonable functional form for the adiabatic elastic constants is

$$C^{ad}_{ik,jl} = \tilde{C}_{ik,jl} - \frac{B^{T}_{ik,jl}}{e^{T_e/T} - 1} + B^{P}_{ik,jl}P. \quad (2)$$

T_e is the effective Einstein temperature, and $B^{T}_{ik,jl}$ and $B^{P}_{ik,jl}$ are coefficients for the temperature and pressure dependence, respectively. We can relate the adiabatic elastic constants to the isothermal elastic constants, $C^{\text{iso}}_{ik,jl}$ through the expression [21]

$$C^{ad}_{ik,jl} - C^{\text{iso}}_{ik,jl} = A_{ik,jl}TC_v. \quad (3)$$

C_v is the specific heat at constant volume, and $A_{ik,jl}$ is a constant of proportionality. Due to the lack of an explicit form for C_v and knowledge of its dependence on pressure, we restrict the current study to the adiabatic elastic constants.

Equation (2) is developed for a solid material and does not consider any transition phenomena. Near the glass transition temperature, the internal relaxation time becomes very sensitive to temperature and the solid glassy state begins to transition into the supercooled liquid regime. It is at this point that the elastic response becomes time-dependent and the frequency at which the measurement is taken must be considered. In this manuscript we focus on isochronal measurements of the elastic response and thus choose the "high-frequency" shear modulus as the value that quantifies the elastic shear response of our MG. By high-frequency we mean that the elastic response does not change beyond a certain fixed frequency. Near the glass transition temperature, the high-frequency shear modulus of the equilibrium supercooled liquid continues to decrease and shows a rate of decay nearly an order of magnitude greater than in the glassy state regimes [9,28,29]. Several functional forms to describe the shear modulus of the equilibrium supercooled liquid have been previously proposed, including an exponential, a power-law, and hyperbolic tangent decay [9,29–31]. Several groups have noted the importance of the shear modulus in the mechanical and thermal properties of metallic glasses and its correlation to the glass transition phenomenon [29,32–35]. In contrast to the shear modulus, it has been noted by several groups that the bulk modulus typically shows a significantly reduced softening effect near the glass transition as compared to the shear modulus [10,29].

Here we are concerned with the continuous transition from the glassy state to the supercooled liquid as the solid assumption begins to break down. To account for an observed increased softening in elastic properties, we modify Eq. (2) as

$$C_{ik,jl} = \left(\tilde{C}_{ik,jl} - \frac{B^{T}_{ik,jl}}{e^{T_e/T} - 1} + B^{P}_{ik,jl}P\right)\Gamma_{ik,jl}(T,P), \quad (4)$$

where Γ is a continuous, monotonically decreasing function that represents the transition. Note that we are chiefly concerned with capturing the continuous nonlinear transition regime and do not presume a functional form of the shear modulus within the equilibrium supercooled liquid although we do require that Γ reproduce the observed sharp increase in decay of the shear modulus. A simple function that meets requirements of continuity, monotonicity, and rapidly increasing rate of decay is the sigmoidal function. In this model, we set $\Gamma = \frac{1}{1+(\frac{T}{T_0(P)})^{z(P)}}$, where T_0 is the inflection point of the sigmoid and z is a positive value that represents the strength of the transition. This general approach allows us to capture the behavior of the transition.

A few comments should be made concerning the choice of T_0 and z in the $\Gamma(T,P)$ function. Within experimental time scales, the glass transition is a kinetic transition and the measured calorimetric glass transition temperature is known to depend on heating rate [36] and molecular dynamic simulations have shown a pressure dependence of the glass transition temperature [19,37] with increases of up to 20 K per magnitude of heating rate or GPa of applied pressure. It is therefore reasonable to expect that the transition parameters will be dependent upon pressure.

Considered as an isotropic solid, the elastic behavior of a BMG can be entirely characterized by two parameters. The most experimentally relevant moduli are the shear and bulk modulus. Following the discussion above, we write

$$\mu(T,P) = \left(\mu_0 - \frac{B^{T}_{\mu}}{e^{T_e/T} - 1} + B^{P}_{\mu}P\right)\frac{1}{1+\left(\frac{T}{T_0(P)}\right)^{z(P)}}, \quad (5)$$

$$K(T,P) = K_0 - \frac{B^{T}_{K}}{e^{T_e/T} - 1} + B^{P}_{K}P. \quad (6)$$

III. MODEL COMPARISON

To validate the ability of Eqs. (5) and (6) to capture the pressure- and temperature-dependent nature of the elastic constants over the relevant temperature and pressure range, we compare them to experimentally reported behavior as well as simulated elastic data over a pressure and temperature range currently inaccessible experimentally.

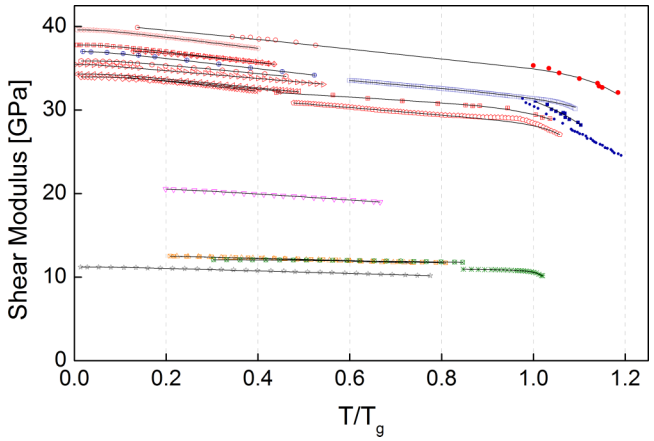

FIG. 1. Experimental data for BMGs: $Zr_{41.2}Ti_{13.8}Cu_{12.5}Ni_{10}Be_{22.5}$ ([23]), $(Cu_{50}Zr_{50})_{95}Al_5$ ([23]), $Zr_{46.75}Ti_{8.25}Cu_{7.5}Ni_{10}Be_{27.5}$ ([29] /), $Zr_{52.5}Cu_{17.9}Ni_{14.6}Al_{10}Ti_5$ ([38]), $Cu_{47.5}Zr_{47.5}Al_5$ ([38]), $Zr_{50}Cu_{40}Al_{10}$ ([38]), $Zr_{50}Cu_{30}Ni_{10}Al_{10}$ ([38]), $Cu_{60}Zr_{30}Ti_{10}$ ([24]), $Cu_{60}Hf_{25}Ti_{15}$ ([24]), $Zr_{55}Cu_{30}Al_{10}Ni_5$ ([39]), $Zr_{55}Cu_{30}Al_{10}Ni_5$ ([40]), $Pd_{42.5}Ni_{7.5}Cu_{30}P_{20}$ ([41]), $Pd_{40}Cu_{30}Ni_{10}P_{20}$ ([42], [43]), $Pd_{43}Ni_{10}Cu_{27}P_{20}$ ([9]), $Mg_{65}Cu_{25}Gd_{10}$ ([23]), $La_{68}Al_{10}Cu_{20}Co_2$ ([23], [25]), $Ce_{68}Al_{10}Cu_{20}Co_2$ ([10], [25]), $Ca_{65}Mg_{15}Zn_{20}$ ([38]) with solid line indicating model fit.

A. Experimental Dataset Comparison

Figure 1 shows a plot of the experimentally measured shear modulus against temperature normalized to the reported calorimetric glass transition temperature for many different BMG systems. Also shown in Fig. 1 are the analytic curves of Eq. (5) fit to each set of experimental data. We refer the reader to the Appendix for a detailed discussion of the fitting procedure. Here we have included several Zr-Cu-dominated [23,24,29,38–40], PdCuNiP [9,26,41–43], $La_{68}Al_{10}Cu_{20}Co_2$ [23,25], $Mg_{65}Cu_{25}Gd_{10}$ [23], $Ca_{65}Mg_{15}Zn_{20}$ [38], and $Ce_{68}Al_{10}Cu_{20}Co_2$ [10,25] BMGs. The vast majority of elastic properties are measured at room and cryogenic temperatures while fewer studies of the high-temperature elastic shear behavior of BMGs are available in the literature due to the difficult nature of such experiments. *In situ* high temperature mechanical measurement techniques used in the work cited here include the pulse echo overlap method [10,39,40] and the contactless electromagnetic acoustic transformation (EMAT) method [42,43]. Techniques such as EMAT can achieve frequencies up to 10 MHz, allowing for the instantaneous mechanical response to be measured. There have also been attempts to characterize the high-temperature mechanical properties *ex situ* by rapidly quenching a fully annealed sample to capture the high-temperature atomic configuration [9,29]. This allows measurements to be performed at room temperature and correcting for thermal expansion gives the high-temperature modulus. We note that near the glass transition, the BMG displays an anelastic response [44,45]. Due to the kinetic nature of the glass transition, the mechanical response of the glassy sample near the transition is expected to be dependent upon pressure and also on the timescale of the mechanical measurement. The time-dependent nature of the mechanical response in glassy materials is most clearly seen in dynamic testing. A recent work by Hecksher *et al.* [46], shows experimental dynamic mechanical testing data for the glass-forming tetramethyl tetraphenyl trisiloxane across a wide range of temperatures and testing frequencies. Such frequency scanning methods are in contrast to experimental data included here that includes only a single measurement frequency. The data presented in Ref. [46] demonstrates that the point at which they observe a drop in storage modulus depends both on temperature and testing frequency. Thus, the fitting parameters T_0 and z included in Eq. (5) are expected to be dependent both on temperature and time scale. In the work presented here, we analogously consider only a single frequency (the high-frequency plateau region in dynamic tests) for the simulated data and experimental data is reported at for a single testing frequency.

In Fig. 1, equilibrium values are indicated by filled symbols, while nonequilibrium data are indicated by unfilled symbols. Temperature data are normalized by the reported glass transition temperature except for one data-set [43], which has been normalized against the reported cross-over temperature of equilibrium data [42].

Figure 1 shows that from $0.2T_g$ up to slightly below T_g, the temperature dependence of the shear modulus is approximately linear. Well above the effective Einstein temperature and below the glass transition temperature, Eq. (5) can be approximated as linear with the slope $\sim -\frac{B_\mu^T}{T_e}$. Below $0.2T_g$, the slope increases to zero as the temperature approaches the effective Einstein temperature and the shear modulus levels off to μ_0. Slightly below T_g, the slope begins to decrease drastically. Due to the increased relaxation time at elevated temperatures, *in situ* measurements of the shear modulus near the glass transition are expected to depend upon the heating rate [45]. This has been demonstrated in $Pd_{40}Cu_{30}Ni_{10}P_{20}$ [43] and the reported equilibrium and nonequilibrium data are included for comparison in Fig. 1.

Figure 1 shows that Eq. (5) is able to fully capture the temperature dependence of the shear modulus of many different BMG systems from the nonlinear cryogenic temperature range, through the linear room temperature regime, and slightly above the glass transition temperature into the supercooled liquid regime. It is also able to capture both equilibrium data and measurements taken at constant heating rate.

Please refer to the Supplemental Material [47] for Table S1, which gives the fitting parameters for all data sets shown in Fig. 1. It is seen that BMGs span a wide range of shear modulus although there is a low variation in the temperature dependence at moderate temperatures. Most BMGs shown here display a room temperature slope between -5 to $-10\,\mathrm{MPa\,K^{-1}}$, showing a moderate temperature dependence. For data passing through the glass transition, T_0 and z are seen to be consistent among similar alloy compositions. Since Γ represents the transition from glassy state to supercooled liquid, T_0 and z are expected to be related to the fragility [9].

The choice of transition function will certainly determine the magnitude of the chosen transition parameters, here T_0 and z. Johnson *et al.* have derived a functional form for the shear modulus of the supercooled liquid [9]. As a check of the magnitude of the parameters we introduce here, we can compare the

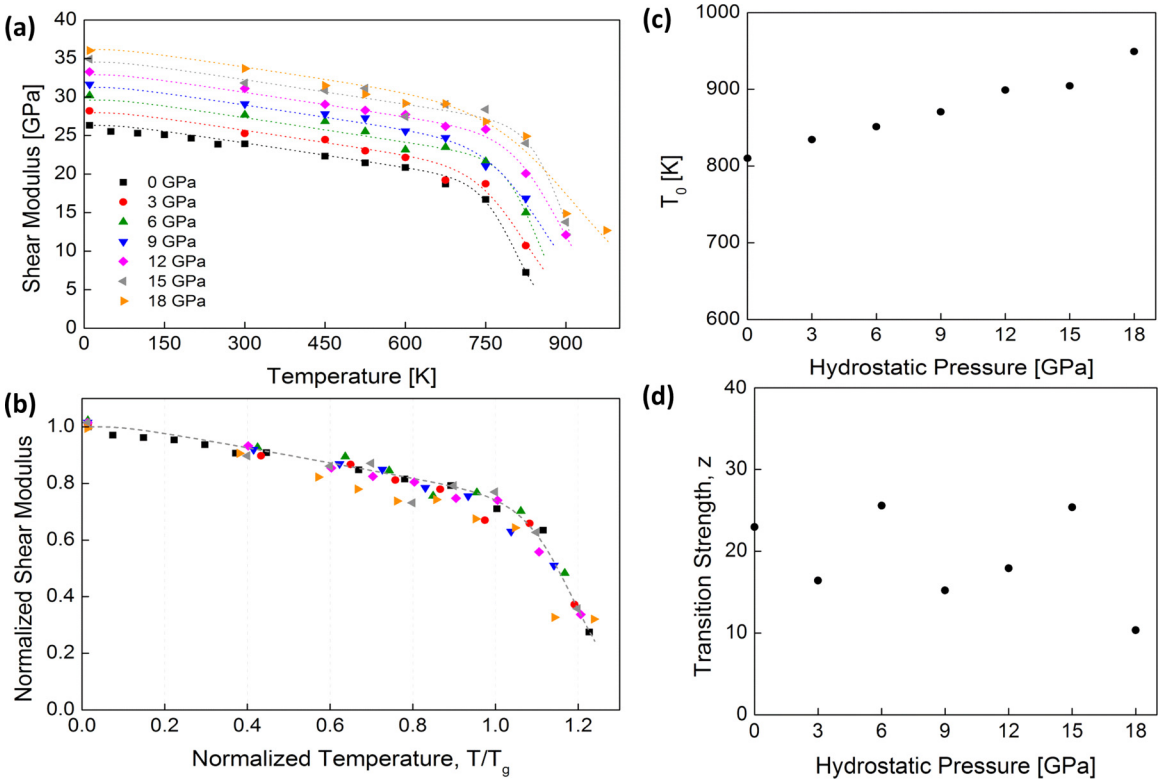

FIG. 2. (a) Shear modulus for the simulated $Cu_{64}Zr_{36}$ as a function of temperature. Each curve shows the dependence for a given applied pressure. Dashed lines indicate the fit curve following Eq. (5). (b) Displays the shear modulus normalized as given in Eq. (7) against the normalized temperature. By accounting for the pressure contribution to the shear modulus and pressure-dependent transition temperature, the shear modulus data all collapse onto a similar curve. The pressure dependence of the glass transition temperature (c) and the strength of the transition (d).

analytic slope of our predicted shear modulus against their prediction for the shear modulus of a supercooled liquid evaluated at T_g. For VIT4, $Pd_{43}Ni_{10}Cu_{27}P_{20}$, and $Pt_{57.5}Ni_{5.3}Cu_{14.7}P_{22.5}$ metallic glasses, the value of $\frac{\partial\mu}{\partial T}|_{T=T_g}/\mu(T_g)$ (as derived from Eq. (11) in Ref. [9]) is $-0.00116\ K^{-1}$, $-0.002\ K^{-1}$, and $-0.0026\ K^{-1}$, respectively. Calculating the same value using Eq. (5) in our manuscript and parameters for VIT4, $Pd_{40}Cu_{30}Ni_{10}P_{20}$, and our simulated $Cu_{64}Zr_{36}$, we find similar values of $-0.0014\ K^{-1}$, $-0.0026\ K^{-1}$, and $-0.0013\ K^{-1}$, respectively. This suggests that the magnitude of these parameters is appropriate for our choice of transition function.

B. Simulated Dataset Comparison

There are few studies of the effect of pressure on the elastic constants of BMGs and none explore the temperature dependence of pressure sensitivity. Figure 2(a) shows the temperature and pressure dependence of the shear modulus as calculated from molecular dynamics simulations of a $Cu_{64}Zr_{36}$ metallic glass. (For details about the simulation procedure and results, please see the Appendix). Values for B_μ^T, T_e, and μ_0 were obtained using a similar fitting procedure as applied to the experimental datasets and B_μ^P was obtained from data calculated at $T = 300\ K$. The behavior of the simulated BMG can then be captured at elevated temperatures and pressures from these low-temperature values. Transition parameters were again obtained using a least square fit procedure. Dashed lines in Fig. 2(a) correspond to the model and show excellent agreement with the simulated data. Figures 2(c) and 2(d) give T_0 and z as a function of applied hydrostatic pressure. The transition temperature appears to linearly increase with pressure while z appears to be weakly dependent on pressure. Motivated by these fittings, we normalize Eq. (5) as

$$\bar{\mu}(\bar{T}) = \frac{\mu(P,\bar{T})}{\mu_o} - \frac{\bar{B}_\mu^P}{1+\left(\frac{\bar{T}}{\bar{T}_0}\right)^z}$$
$$P = \left(1 - \frac{\bar{B}_\mu^T}{e^{\frac{\bar{T}_e}{\bar{T}}}-1}\right)\frac{1}{1+\left(\frac{\bar{T}}{\bar{T}_0}\right)^z}, \tag{7}$$

where $\bar{T} = \frac{T}{T_g}$, $\bar{T}_e = \frac{T_e}{T_g}$, $\bar{T}_0 = \frac{T_0}{T_g}$, $\bar{B}_\mu^T = \frac{B_\mu^T}{\mu_o}$, and $\bar{B}_\mu^P = \frac{B_\mu^P}{\mu_o}$. Figure 2(c) gives a pressure dependence for T_0 of ~ 7 K GPa^{-1}, which corresponds well with the previously reported pressure dependence of the crystallization temperature of $Pd_{40}Cu_{30}Ni_{10}P_{20}$ [17] at 11 K GPa^{-1} and pressure dependence of the glass transition temperature of $Zr_{46.8}Ti_{8.2}Cu_{7.5}Ni_{10}Be_{27.5}$ [18] and $Cu_{50}Zr_{50}$ [19] systems at 4.4 K GPa^{-1}, and 14 K GPa^{-1}, respectively. This suggests that the ratio $\frac{T_0}{T_g}$ should be weakly dependent on hydrostatic pressure. For the glass transition temperature under no applied pressure obtained from simulations ($T_g = 670$ K), we then take the value $\bar{T}_0 = 1.2$, consistent with values reported in Table S1. Figure 2(b) shows that by normalizing through Eq. (7), all simulated shear modulus data collapse onto the same curve as

a function of normalized temperature. With the exception of the highest values of pressure, the shear modulus data as shown in Fig. 2(b) differs only by a few percent from the normalized curve.

Figures 1 and 2 show that Eq. (5) is able to capture the behavior of the shear modulus from low temperatures through the glass transition temperature and under a hydrostatic pressure. The normalized shear modulus decreases approximately linearly until the glass transition temperature, after which it begins to drop precipitously. In the solid glassy state, the assumptions of the quasiharmonic theory remain valid. Near the glass transition where these assumptions begin to break down, the Γ function can then be said to dominate the behavior of the shear modulus. Combined with the observations of a linear dependence of glass transition temperature, this suggests that hydrostatic pressure chiefly acts to shift the transition regime to higher temperatures by constraining atomic motion [37]. This is demonstrated in the normalized temperature, $\bar{T} = \frac{T}{T_g(P)}$, where we see that even a small hydrostatic pressure can significantly change the position along the normalized curve as shown in Fig. 2(b). Further, the sensitivity of the normalized temperature with respect to pressure increases with increasing temperature. Analogous to thermal quenching, an applied pressure can result in movement from the supercooled liquid regime ($\bar{T} > 1$) to the glass regime ($\bar{T} < 1$). Such increasing pressure sensitivity of the mechanical behavior of metallic glasses near the glass transition temperature has been observed experimentally [16].

We should note that values of shear modulus shown in Fig. 2(b) are taken from a single simulation sample due to the high computational cost in creating metallic glass samples through simulated quenching. Due to the nonergodic nature of metallic glass, the existence (or lack thereof) of coupling between pressure and temperature dependence of the shear modulus at high temperatures may be made clearer with the inclusion of further simulation and study.

Figure 3(a) shows the temperature and pressure dependence of the bulk modulus as calculated from molecular dynamics simulations. Dashed lines in Fig. 3(a) correspond to the model and show excellent agreement with Eq. (6). Following the procedure used for the shear modulus, Eq. (6) can be normalized as

$$\bar{K}(\bar{T}) = \frac{K(P,\bar{T})}{K_o} - \bar{B}_K^P P = 1 - \frac{\bar{B}_K^T}{e^{\bar{T}_e/\bar{T}} - 1}, \qquad (8)$$

where $\bar{B}_K^T = \frac{B_K^T}{K_o}$ and $\bar{B}_K^P = \frac{B_K^P}{K_o}$. Figure 3(b) shows that normalizing through Eq. (8) results in a collapse of the bulk modulus data. It has been noted previously that the bulk modulus displays an approximate linear dependence on hydrostatic pressure [7,15], which is predicted by Eq. (6) for a fixed temperature.

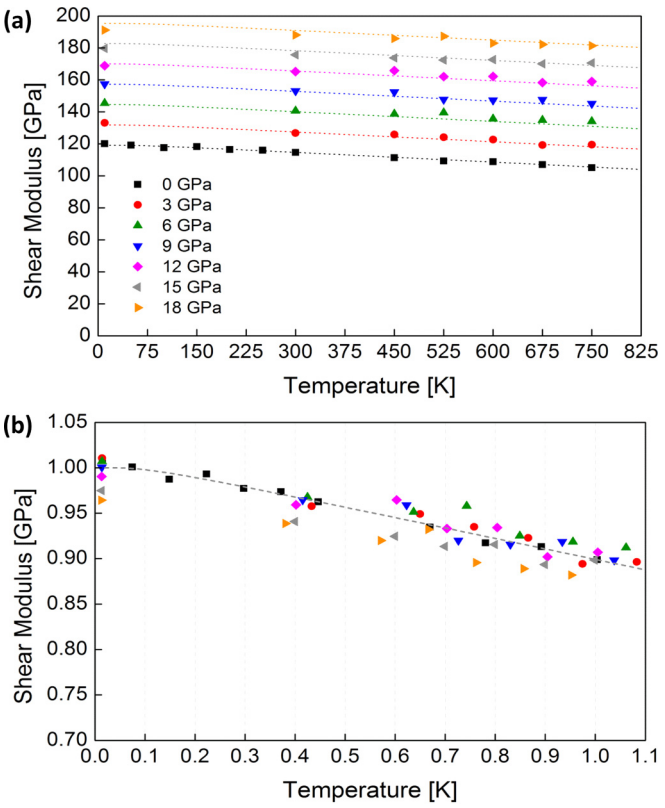

FIG. 3. (a) The bulk modulus as a function of temperature. Each curve shows the dependence for a given applied pressure. Dashed lines indicate the fit curve following Eq. (6). The bulk modulus decreases weakly with temperature while showing a significant dependence on the applied pressure. (b) The bulk modulus normalized as indicated in Eq. (8) plot against the normalized temperature. Accounting for the pressure contribution to the bulk modulus results in a collapse of the bulk modulus data onto a similar curve.

IV. DISCUSSION

All fitting parameters for the simulated elastic constants are given in Table S2. Comparing the values $\frac{\bar{B}_\mu^T}{\bar{B}_K^T} = 2.55$ and $\frac{\bar{B}_\mu^P}{\bar{B}_K^P} = 0.58$ indicate that the shear modulus is more than twice as sensitive to changes in temperature as the bulk modulus while ~40% less sensitive to changes in pressure. Interestingly, the normalized values of pressure sensitivity for the shear modulus, $\bar{B}_\mu^P = 0.0217$, and bulk modulus, $\bar{B}_K^P = 0.0335$, reported here are quantitatively similar to the pressure sensitivities reported for Vit 1 (0.0203 and 0.0351) [13], $Cu_{60}Zr_{20}Hf_{10}Ti_{10}$ (0.0236 and 0.0421) [48], and $Pd_{39}Ni_{10}Cu_{30}P_{21}$ (0.0222 and 0.0390) [49].

There has been much work investigating the sources of pressure-dependent behavior in nonmetallic, typically polymer and molecular, glassy systems (for example, see the review by Roland *et al.* [50]). Of particular interest is the role of pressure on the behavior of viscosity and relaxation time in a glass-forming liquid. The sources of pressure dependence for these quantities can provide insight into the pressure dependence of mechanical behavior.

Most models describing the pressure and temperature dependence of viscosity are modifications of the Vogel-Fulcher-Tammann (VFT) equation and largely empirical. The physical source of pressure dependence is often described using a variety of measures of "free volume," which generally defines the difference between the total volume and "occupied" volume. This excess or "free" volume allows for atomic rearrangements and would clearly be expected to depend upon an applied hydrostatic pressure. There are important

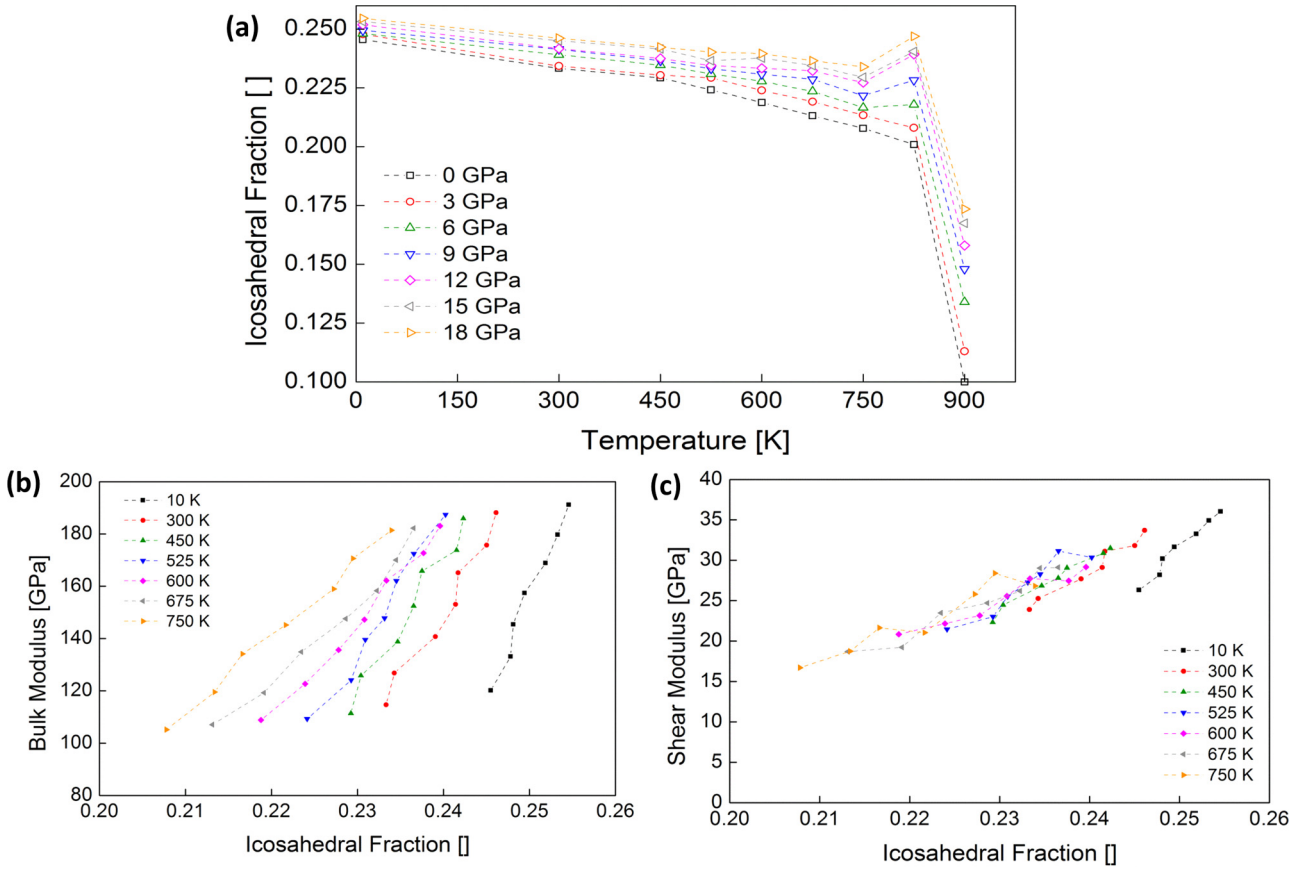

FIG. 4. (a) The dependence of Cu atoms with icosahedral coordination as a function of temperature. Icosahedral coordination generally decreases with increasing temperature and increases with applied pressure. Approaching the glass transition temperature, there is an increase in the sensitivity of icosahedral coordination to applied pressure. (b) Correlation between the bulk modulus and fraction of Cu atoms with icosahedral coordination. The bulk modulus shows less sensitivity to temperature than icosahedral coordination. (c) Correlation between the shear modulus and fraction of Cu atoms with icosahedral coordination. The similar isothermal curves suggest that the shear modulus and icosahedral coordination have similar sensitivities to temperature and pressure.

differences between metallic and nonmetallic glass-forming systems that should be noted. It has been observed that free volume models that have been successful in describing polymer glasses may not be appropriate to metallic systems due to their "soft" core behavior and nondirectional bonding [51].

In spite of a large volume of work to elucidate the microstructural origins of the mechanical behavior in metallic glasses, no conclusive theory has been reached. Many proposed indicators for the internal microstructural state have been motivated by the observation of a significant configurational dependence of the shear modulus [52–56]. By considering both short-range and medium-range contributions to the shear modulus, Ma *et al.* concluded that differences in the medium-range order underlie differences in the shear modulus of $Cu_{50}Zr_{50}$ metallic glasses quenched at different cooling rates [57]. Indeed, the shear modulus is also seen to strongly correlate with the fraction of Cu atoms with icosahedral coordination in Cu-Zr BMG systems [52,58–60]. The configurational dependence of the shear modulus is then seen as a result of ordering of the local atomic clusters into icosahedral coordination and the medium-range order beyond the local clusters. As icosahedral coordination is the energetically preferred local configuration [57], such a process would generally agree well with correlations of configurational potential energy.

Figure 4(a) gives the fraction of Cu atoms with icosahedral coordination as a function of temperature and pressure. Figures 4(b) and 4(c), respectively, show the bulk and shear moduli against the fraction of Cu atoms with icosahedral coordination. Due to microstructural changes caused by relaxation at elevated temperatures as seen in Fig. 4(a), we omit data above 750 K in Figs. 4(b) and 4(c). Figures 4(b) and 4(c) clearly show that there is a strongly positive, linear correlation between the fraction of Cu atoms with icosahedral coordination and the elastic constants. The strong correlation between icosahedral atoms and the shear modulus shown in Fig. 4(c) suggests that to first order in pressure and temperature, icosahedral atoms and the shear modulus have similar pressure and temperature dependencies and it may be prudent to ask whether a similar quasi-harmonic model may also shed light on the dependence of short-range order in the glass. Although it might generally be expected that a denser glass will have a greater fraction of icosahedral atoms, the lack of details of such a correlation means that the fraction of icosahedral atoms cannot be fully captured by the anharmonic dependence of atomic spacing.

While Fig. 4 demonstrates the correlation between short-range order and the shear modulus is observed over a wide range of temperatures and pressures, we might ask to what extent are changes in short-range order the cause of

changes in shear modulus. We may allow that the change in elastic moduli can have a contribution due to anharmonicity and some contribution due to "structural changes" (athermal term). We have performed annealing by bringing the sample to a temperature of 825 K and holding it there for 3 ns. We then quench it back down to 300 K using a quench rate of 10^{10} Ks^{-1}. This results in an increase in the icosahedral fraction from 23.3% to 27.0% showing a significant amount of structural relaxation has taken place. The temperature pathway and evolution of icosahedral fraction is shown in Fig. S1 [47]. Despite this, the shear modulus calculated before annealing was 23.9 GPa and the shear modulus calculated after the annealing took place was 23.2 GPa. This suggests that any structural changes that may occur (whether it is local, reversible β-relaxation or long-range, irreversible α-relaxation) do not play a significant part in the temperature and pressure dependence of the elastic moduli and that the anharmonic nature of the interatomic potential is the primary source of the temperature and pressure dependence.

There is currently no widely accepted model that connects icosahedral coordination and the mechanical properties of metallic glasses although a more general result has shown that Cu atoms with icosahedral coordination exhibit more resistance against local shear deformation [61,62]. Icosahedral short-range order is most likely not the singular microstructural motif that determines mechanical properties as demonstrated by the strong correlation between the bulk and shear moduli with other top, most populous low-energy, high-density atomic configurations as shown in Figs. S2, S3, and S4 [47]. It has been shown more generally that fivefold symmetries are correlated with relaxation in glasses [63–66], and thus the correlations shown in Figs. 4(b) and 4(c) (together with Figs. S2, S3, and S4) demonstrate the correlation between elastic properties and fivefold coordination symmetry.

V. CONCLUSION

We have presented an anharmonic model to account for both the temperature and pressure dependence of the elastic properties in a representative BMG. We have demonstrated that the model is able to capture the reported temperature and pressure dependence of the elastic properties of many BMGs across a wide range of temperatures and hydrostatic pressures. Consistent with previous experimental results, the effect of pressure shifts the glass transition to higher temperatures, effectively extending the solid regime. We have also verified the correlation between icosahedral short-range order and the elastic moduli under varied pressure and temperature. The effects of pressure and temperature and the origin of temperature-dependent pressure-sensitivity as revealed here have significantly expanded our understanding about the physical origins of mechanical properties in BMGs. The origin revealed here for the experimentally observed pressure behavior in BMGs is of importance toward identifying fabrication and processing paths for metallic glass components [67] as well as gaining deeper insight into the glass transition phenomenon.

ACKNOWLEDGMENTS

The authors gratefully acknowledge the financial support from the Agency for Science, Technology and Research (A*STAR), Singapore, and the use of computing resources at the A*STAR Computational Resource Centre, Singapore. Support for one of the authors (J.J.L.) was provided by the Arthur P. Armington Professorship at CWRU.

APPENDIX: SIMULATION METHODS AND MODEL FITTING

We employ molecular dynamic simulations to compare the current model to elastic behavior under high pressure and temperature. To construct the initial sample, rapid quenching was simulated using the LAMMPS molecular dynamics software [68]. The system consisted of 8000 atoms using a $Cu_{64}Zr_{36}$ composition, a good glass former that has been previously well-characterized [69,70]. From an initially random cubic configuration with fully periodic boundary conditions, the system was assigned a velocity profile that corresponded to 2000 K, well above the expected melting temperature ($\sim$1300 K) [71]. The system was held at 2000 K and stress-free boundary conditions for 1 ns using an integration timestep of 1 fs. This was followed by a quench down to 10 K at a rate of 10^{10} Ks^{-1} under stress-free boundary conditions. Following quenching, the base sample was then brought to temperatures ranging from 10 to 1050 K. At each temperature, we generated two sample sets by applying a simulation pressure ranging from 0 to 18 GPa following both an adiabatic (NVE ensemble) and isothermal (NPT) path. This resulted in a dense mesh of the parameter space that covered temperatures from near 10 K through the glass transition regime and hydrostatic pressures up to 75% of the room temperature shear modulus. For each sample, we calculated the bulk and shear modulus. The bulk modulus was defined as

$$K = -V\frac{dP}{dV}. \tag{A1}$$

We performed shearing simulations by applying a shear strain to the simulation box at a strain rate ranging from $0.7 \cdot 10^6$ s^{-1} to 10^9 s^{-1}. The shear modulus was calculated as the slope of the initial linear regime of the stress-strain data. Bulk modulus data presented here was taken from the adiabatic sample set while shear modulus data was taken from the isothermal sample set which we note should be equivalent to the adiabatic shear modulus. For consistency and to allow for a reliable fit, we took the linear regression up to 0.025 shear strain, well below the typically observed onset of plasticity at $\sim$0.05. Below the glass transition temperature, the shear modulus as calculated using this procedure does not differ significantly as a function of strain rate. In contrast, above the glass transition temperature, the shear modulus was observed to decrease by as much as 44% when the strain rate was decreased from 10^8 s^{-1} to 0.7×10^6 s^{-1}. In contrast, increasing the strain rate from 10^8 s^{-1} to 10^9 s^{-1} shows no significant or consistent change in the shear modulus. Based on this observation, we take the shear modulus as calculated here

to be the "instantaneous" elastic response of the material. The modulus as reported in the manuscript was calculated using data from dynamic simulations performed at 10^8 s^{-1}. Under an assumption of material isotropy, all other material properties were defined from the calculated shear and bulk moduli.

Radical Voronoi analysis was performed using Voro++ software library [72] using atomic radii of 1.28 and 1.59 Å for Cu and Zr, respectively.

Solid lines in Fig. 1 show the fit of Eq. (5) to the experimental data. For all data sets, an important and easily obtained value is the slope at room temperature, which can be approximated as $\frac{\partial \mu}{\partial T}|_{T=T_{\mathrm{RT}}} = \mu'_{\mathrm{RT}} \approx -\frac{B_\mu^T}{T_e}$. Evaluating Eq. (5) at room temperature, T_{RT}, and cryogenic temperature, T_{cryo}, and taking the difference between the two gives

$$0 = \mu(T_{\mathrm{cryo}}) - \mu(T_{\mathrm{RT}}) + \frac{B_\mu^T}{e^{-\frac{B_\mu^T}{\mu'_{\mathrm{RT}} T_{\mathrm{cryo}}}} - 1} - \frac{B_\mu^T}{e^{-\frac{B_\mu^T}{\mu'_{\mathrm{RT}} T_{\mathrm{RT}}}} - 1}, \tag{A2}$$

which can be used to obtain B_μ^T from the experimental data. T_e is then immediately obtained from the room temperature slope, μ'_{RT} and similarly, μ_0 is then specified from these two constants and any point in the dataset. For high temperature data sets, we use the value of T_e obtained at low temperature and obtain B_μ^T from the room temperature slope. These three parameters quantify the glassy response of the bulk metallic glass and the transition parameters can then be obtained from least squares fit.

[1] A. L. Greer and E. Ma, MRS Bull. **32**, 611 (2007).
[2] C. Suryanarayana and A. Inoue, *Bulk Metallic Glasses* (CRC Press, Boca Raton, FL, 2010).
[3] M. D. Demetriou, M. E. Launey, G. Garrett, J. P. Schramm, D. C. Hofmann, W. L. Johnson, and R. O. Ritchie, Nat. Mater. **10**, 123 (2011).
[4] X. J. Gu, S. J. Poon, G. J. Shiflet, and J. J. Lewandowski, Acta Mater. **58**, 1708 (2010).
[5] S.-W. Lee, M. Jafary-Zadeh, D. Z. Chen, Y.-W. Zhang, and J. R. Greer, Nano Lett. **15**, 5673 (2015).
[6] M. Jafary-Zadeh, R. Tavakoli, D. J. Srolovitz, and Y.-W. Zhang, Extrem. Mech. Lett. **9**, 215 (2016).
[7] W. H. Wang, Prog. Mater. Sci. **57**, 487 (2012).
[8] G. Kumar, H. X. Tang, and J. Schroers, Nature **457**, 868 (2009).
[9] W. L. Johnson, M. D. Demetriou, J. S. Harmon, M. L. Lind, and K. Samwer, MRS Bull. **32**, 644 (2007).
[10] B. Zhang, H. Y. Bai, R. J. Wang, Y. Wu, and W. H. Wang, Phys. Rev. B **76**, 012201 (2007).
[11] P. Lowhaphandu, S. L. Montgomery, and J. J. Lewandowski, Scr. Mater. **41**, 19 (1999).
[12] J. J. Lewandowski and P. Lowhaphandu, Philos. Mag. A **82**, 3427 (2002).
[13] W. Hua Wang, F. Li, M. Pan, D. Zhao, and R. J. Wang, Acta Mater. **52**, 715 (2004).
[14] W. H. Wang, P. Wen, L. M. Wang, Y. Zhang, M. X. Pan, D. Q. Zhao, and R. J. Wang, Appl. Phys. Lett. **79**, 3947 (2001).
[15] J. Caris and J. J. Lewandowski, Acta Mater. **58**, 1026 (2010).
[16] L. O. Vatamanu and J. J. Lewandowski, Mech. Mater. **67**, 86 (2013).
[17] J. Z. Jiang, Y. X. Zhuang, H. Rasmussen, N. Nishiyama, A. Inoue, and C. Lathe, Europhys. Lett. **54**, 182 (2001).
[18] J. Z. Jiang, W. Roseker, M. Sikorski, Q. P. Cao, and F. Xu, Appl. Phys. Lett. **84**, 1871 (2004).
[19] J. Ding, M. Asta, and R. O. Ritchie, Phys. Rev. B **93**, 140204 (2016).
[20] F. Decremps, G. Morard, G. Garbarino, and M. Casula, Phys. Rev. B **93**, 054209 (2016).
[21] G. Leibfried and W. Ludwig, in *Solid State Phys. XII*, edited by F. Seitz and D. Turnbull (Academic Press, New York, 1961), pp. 275–444.
[22] Y. P. Varshni, Phys. Rev. B **2**, 3952 (1970).
[23] P. Yu, R. J. Wang, D. Q. Zhao, and H. Y. Bai, Appl. Phys. Lett. **90**, 251904 (2007).
[24] R. Tarumi, M. Hirao, T. Ichitsubo, E. Matsubara, J. Saida, and H. Kato, Phys. Rev. B **76**, 104206 (2007).
[25] P. Yu, R. J. Wang, D. Q. Zhao, and H. Y. Bai, Appl. Phys. Lett. **91**, 201911 (2007).
[26] M. Fukuhara, T. Wada, A. Inoue, and F. Yin, Philos. Mag. Lett. **88**, 335 (2008).
[27] M. Fukuhara, X. Wang, A. Inoue, and F. Yin, Phys. Status Solidi Rapid Res. Lett. **1**, 220 (2007).
[28] V. A. Khonik, Y. P. Mitrofanov, S. A. Lyakhov, A. N. Vasiliev, S. V. Khonik, and D. A. Khoviv, Phys. Rev. B **79**, 132204 (2009).
[29] M. L. Lind, G. Duan, and W. L. Johnson, Phys. Rev. Lett. **97**, 015501 (2006).
[30] M. D. Demetriou, J. S. Harmon, M. Tao, G. Duan, K. Samwer, and W. L. Johnson, Phys. Rev. Lett. **97**, 065502 (2006).
[31] J. S. Harmon, M. D. Demetriou, and W. L. Johnson, Appl. Phys. Lett. **90**, 171923 (2007).
[32] J. J. Lewandowski, W. H. Wang, and A. L. Greer, Philos. Mag. Lett. **85**, 77 (2005).
[33] J. C. Dyre, N. B. Olsen, and T. Christensen, Phys. Rev. B **53**, 2171 (1996).
[34] W. L. Johnson and K. Samwer, Phys. Rev. Lett. **95**, 195501 (2005).
[35] S. V. Khonik, A. V. Granato, D. M. Joncich, A. Pompe, and V. A. Khonik, Phys. Rev. Lett. **100**, 065501 (2008).
[36] R. Busch, E. Bakke, and W. L. Johnson, Acta Mater. **46**, 4725 (1998).
[37] Y.-C. Hu, P.-F. Guan, Q. Wang, Y. Yang, H.-Y. Bai, and W.-H. Wang, J. Chem. Phys. **146**, 24507 (2017).
[38] Z. Zhang, V. Keppens, and T. Egami, J. Appl. Phys. **102**, 123508 (2007).
[39] V. Keryvin, T. Rouxel, M. Huger, and L. Charleux, J. Ceram. Soc. Japan **116**, 851 (2008).
[40] T. Ichitsubo, S. Kai, H. Ogi, M. Hirao, and K. Tanaka, Scr. Mater. **49**, 267 (2003).
[41] T. Ichitsubo, E. Matsubara, K. Miyagi, W. Itaka, K. Tanaka, and S. Hosokawa, Phys. Rev. B **78**, 052202 (2008).
[42] Y. P. Mitrofanov, V. A. Khonik, A. V. Granato, D. M. Joncich,

S. V. Khonik, and A. M. Khoviv, Appl. Phys. Lett. **100**, 171901 (2012).
[43] V. A. Khonik, Y. P. Mitrofanov, A. S. Makarov, R. A. Konchakov, G. V. Afonin, and A. N. Tsyplakov, J. Alloys Compd. **628**, 27 (2015).
[44] A. H. Vormelker, O. L. Vatamanu, L. Kecskes, and J. J. Lewandowski, Metall. Mater. Trans. A **39**, 1922 (2008).
[45] J. Lu, G. Ravichandran, and W. L. Johnson, Acta Mater. **51**, 3429 (2003).
[46] T. Hecksher, D. H. Torchinsky, C. Klieber, J. A. Johnson, J. C. Dyre, and K. A. Nelson, Proc. Natl. Acad. Sci. U.S.A. **114**, 8710 (2017).
[47] See Supplemental Material at http://link.aps.org/supplemental/10.1103/PhysRevB.97.014101 for tables containing all fitting parameters for experimental and simulation data. Also included are figures showing correlations between short-range order and the shear and bulk modulus across all simulation pressures and temperatures.
[48] Z. X. Wang, R. J. Wang, and W. H. Wang, Mater. Lett. **60**, 831 (2006).
[49] L. M. Wang, L. L. Sun, W. H. Wang, R. J. Wang, Z. J. Zhan, D. Y. Dai, and W. K. Wang, Appl. Phys. Lett. **77**, 3734 (2000).
[50] C. M. Roland, S. Hensel-Bielowka, M. Paluch, and R. Casalini, Reports Prog. Phys. **68**, 1405 (2005).
[51] T. Egami, JOM **62**, 70 (2010).
[52] J. Ding, Y.-Q. Cheng, and E. Ma, Acta Mater. **69**, 343 (2014).
[53] Y. Q. Cheng, A. J. Cao, and E. Ma, Acta Mater. **57**, 3253 (2009).
[54] G. Duan, M. L. Lind, M. D. Demetriou, W. L. Johnson, W. A. Goddard, III, T. Çağin, and K. Samwer, Appl. Phys. Lett. **89**, 151901 (2006).
[55] S. G. Mayr, Phys. Rev. B **79**, 060201 (2009).
[56] R. Liontas, M. Jafary-Zadeh, Q. Zeng, Y.-W. Zhang, W. L. Mao, and J. R. Greer, Acta Mater. **118**, 270 (2016).
[57] Y. Q. Cheng and E. Ma, Phys. Rev. B **80**, 064104 (2009).
[58] M. Wakeda and Y. Shibutani, Acta Mater. **58**, 3963 (2010).
[59] M. Lee, C.-M. Lee, K.-R. Lee, E. Ma, and J.-C. Lee, Acta Mater. **59**, 159 (2011).
[60] R. Soklaski, V. Tran, Z. Nussinov, K. F. Kelton, and L. Yang, Philos. Mag. **96**, 1212 (2015).
[61] J. Ding, Y. Q. Cheng, and E. Ma, Appl. Phys. Lett. **101**, 121917 (2012).
[62] Y. Q. Cheng, J. Ding, and E. Ma, Mater. Res. Lett. **1**, 3 (2013).
[63] A. Hirata, P. Guan, T. Fujita, Y. Hirotsu, A. Inoue, A. R. Yavari, T. Sakurai, and M. Chen, Nat. Mater. **10**, 28 (2011).
[64] X. K. Xi, L. L. Li, B. Zhang, W. H. Wang, and Y. Wu, Phys. Rev. Lett. **99**, 095501 (2007).
[65] N. Mattern, P. Jóvári, I. Kaban, S. Gruner, A. Elsner, V. Kokotin, H. Franz, B. Beuneu, and J. Eckert, J. Alloys Compd. **485**, 163 (2009).
[66] C. Tang and C. H. Wong, J. Non. Cryst. Solids **422**, 39 (2015).
[67] J. J. Lewandowski and P. Lowhaphandu, Int. Mater. Rev. **43**, 145 (1998).
[68] S. Plimpton, J. Comp. Phys. **117**, 1 (1995).
[69] Y. Q. Cheng, H. W. Sheng, and E. Ma, Phys. Rev. B **78**, 014207 (2008).
[70] Y. Q. Cheng and E. Ma, Prog. Mater. Sci. **56**, 379 (2011).
[71] W. Gierlotka, K.-C. Zhang, and Y.-P. Chang, J. Alloys Compd. **509**, 8313 (2011).
[72] C. H. Rycroft, Chaos Interdiscip. J. Nonlin. Sci. **19**, 41111 (2009).